*16th World Conference on Earthquake Engineering, 16WCEE 2017*
*Santiago Chile, January 9th to 13th 2017*
*Paper N° 4368 (Abstract ID)*
*Registration Code: S- B1462534797*

# SYSTEM IDENTIFICATION AND RESPONSE SIMULATION OF REINFORCED CONCRETE BUILDINGS SEISMICALLY RETROFITTED BY BASE ISOLATION

G. Oliveto[(1)], A. Athanasiou[(2)], A. Markou[(3)], G. Marino[(4)] , N. D. Oliveto[(5)]

[(1)] *Professor, University of Catania, goliveto@dica.unict.it*
[(2)] *Postdoctoral researcher, University of Catania, athanasiou@dica.unict.it*
[(3)] *PhD, Civil Engineer, athanasiosmarkou@gmail.com*
[(4)] *Civil Engineer, giovannim@alice.it*
[(5)] *PhD, Civil Engineer, e-mail: noliveto@buffalo.edu*

## *Abstract*

The dynamic identification of a four story reinforced concrete building retrofitted by base isolation is performed on the basis of push and release tests performed on the building. The identification is performed in two stages. In the first stage, the superstructure is considered rigid and the isolation system is identified by using a tri-linear model for the high damping rubber bearings and a constant Coulomb friction model for the low friction sliding bearings. In the second stage, the motion recorded just above the isolation system is considered as the input of a detailed free-body SAP2000 model of the superstructure. For identification purposes, a condensed model is derived from the detailed model. This is used in combination with the Covariance Matrix Adaptation-Evolution Strategy (CMA-ES) optimization algorithm for the identification of the structural parameters consisting of a multiplier of the stiffness matrix and a parameter specifying stiffness proportional damping. The identified model parameters are used for the simulation of the experimental recorded accelerations and the match is quite satisfactory. The use of the identified parameters for the isolation system and for the superstructure in the detailed SAP2000 model produces results that match the general trend of the isolation mode but fail to reproduce the high frequency response exhibited by the experimental results. The reaction history of the isolation system on the superstructure is evaluated by using both the rigid superstructure model and the one considering deformation of the superstructure. It is shown that while the former does not exhibit high frequency content, the latter shows considerable high frequency response. Application of the reaction containing high frequency components to the detailed SAP2000 model results in accelerations that match reasonably well the experimentally measured ones. Finally, the identified stiffness parameters point towards a significant reduction of the modulus of elasticity of concrete for the evaluation of the cross section rigidities when using gross section second order moments of inertia. The significant identified damping ratios appear to be considerably large consistent with the large released force and resulting initial acceleration and subsequent rapid attenuation.

*Keywords: base isolation; dynamic testing; structural identification; numerical simulation; non-linear behavior*

## 1. Introduction

Around the turn of the century, two four-story reinforced concrete buildings in the town of Solarino in Eastern Sicily, Fig. 1, were retrofitted against seismic excitation using base isolation. Upon completion of the retrofitting works in July 2004, one of the buildings (civic number 25, to the right in Fig.1) was subjected to free vibration tests by application and sudden release of the design displacement [1, 2]. The building was instrumented so as to record the accelerations of the six rigid body modes plus those associated with the deformation modes, Fig. 2. Transducer 07 at station S2 was oriented in the transverse direction (Y) in tests 1 to 5, and in the longitudinal direction (X) in tests 6 to 8. A simple model was then used to identify the properties of the base isolation system [3]. Subsequently, an analytical solution was provided for the simulation of the dynamic response of the base isolation system under earthquake excitation [4]. Finally, a numerical constrained optimization procedure was provided as an alternative to the analytical solution in view of applications to 2D ground motion excitation [5, 6]. All previous studies aiming at model parameter identification and response simulation of the seismic isolation system were based on considering the superstructure as a rigid body. The aim of the present contribution is to

Fig. 1 – The two IACP buildings seismically retrofitted by base isolation in Via Baden Powell 23-25, Solarino, Syracuse, Sicily.

consider the deformation of the superstructure and to pursue model identification of the global system consisting of isolation system and superstructure. The present goal will be pursued with a two-stage strategy. In the first stage, the superstructure will be considered rigid and a single set of model parameters for the isolation system will be derived from the full set of free vibration tests conducted in 2004. In the second stage, the superstructure will be taken as a deformable body and identified by applying the acceleration recorded just above the isolation system, and using the acceleration recorded on the upper floors as identification data. Finally, the global identified model will be used for the simulation of the response of the base-isolated building to seismic excitation.

## 2. Identification of the base isolation system

The layout of the isolation system of the Solarino buildings can be found in [1, 2, 4]. The system is composed of 12 high damping rubber bearings (HDRBs) and 13 low friction sliding bearings (LFSBs). The presence of stiffening walls in the superstructure, as shown in [1], makes the hypothesis of rigid superstructure very realistic and particularly useful for the identification of the properties of the isolation system. For the identification of the HDRB component of the isolation system, the bi-linear hysteretic model (BHM) has been initially used [3, 4, 5, 6]. At a later stage, improved results were obtained by using a tri-linear hysteretic model (THM) [7, 8]. In the works quoted above, each test was used for independent identifications and produced independent sets of identified parameters. In the present work, tests 3, 5, 6, 7, 8 [2, 7] are used together to produce a single set of identified parameters. The LFSB component of the isolation system has been identified initially by using a constant Coulomb friction model (CCFM) [3], and later by using a linear Coulomb friction model (LCFM) [4, 6, 7].

Two sets of identified parameters, obtained from all the considered tests, are shown in Table 1. The first set was obtained by using the THM, while the second one was obtained by using the BHM. Among the identified parameters is also the initial imposed displacement, which was different for each test. As expected, the two considered models, i.e. the THM and the BHM, provide different estimates of the initial displacements $u_0$. The parameters associated with the LFSBs are $u_{d0}$ and $r_{d0}$ [7, 8]; the first is a measure of the friction force at zero displacement, while the second is a specification of the slope of the force-displacement curve. The parameters associated with the HDRBs are the first and second yield displacements, $u_y$ and $u_B$, and the three characteristic frequencies of the system, $f_0$, $f_1$ and $f_2$ [7, 8].

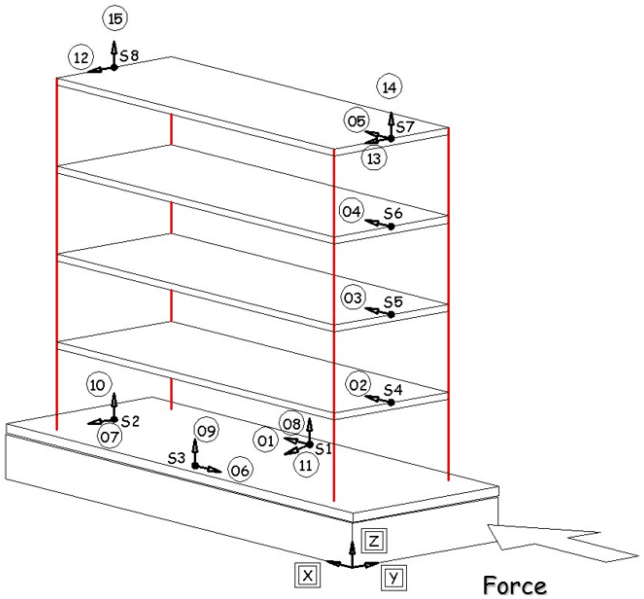


Fig. 2 - Schematic layout of acceleration transducers.

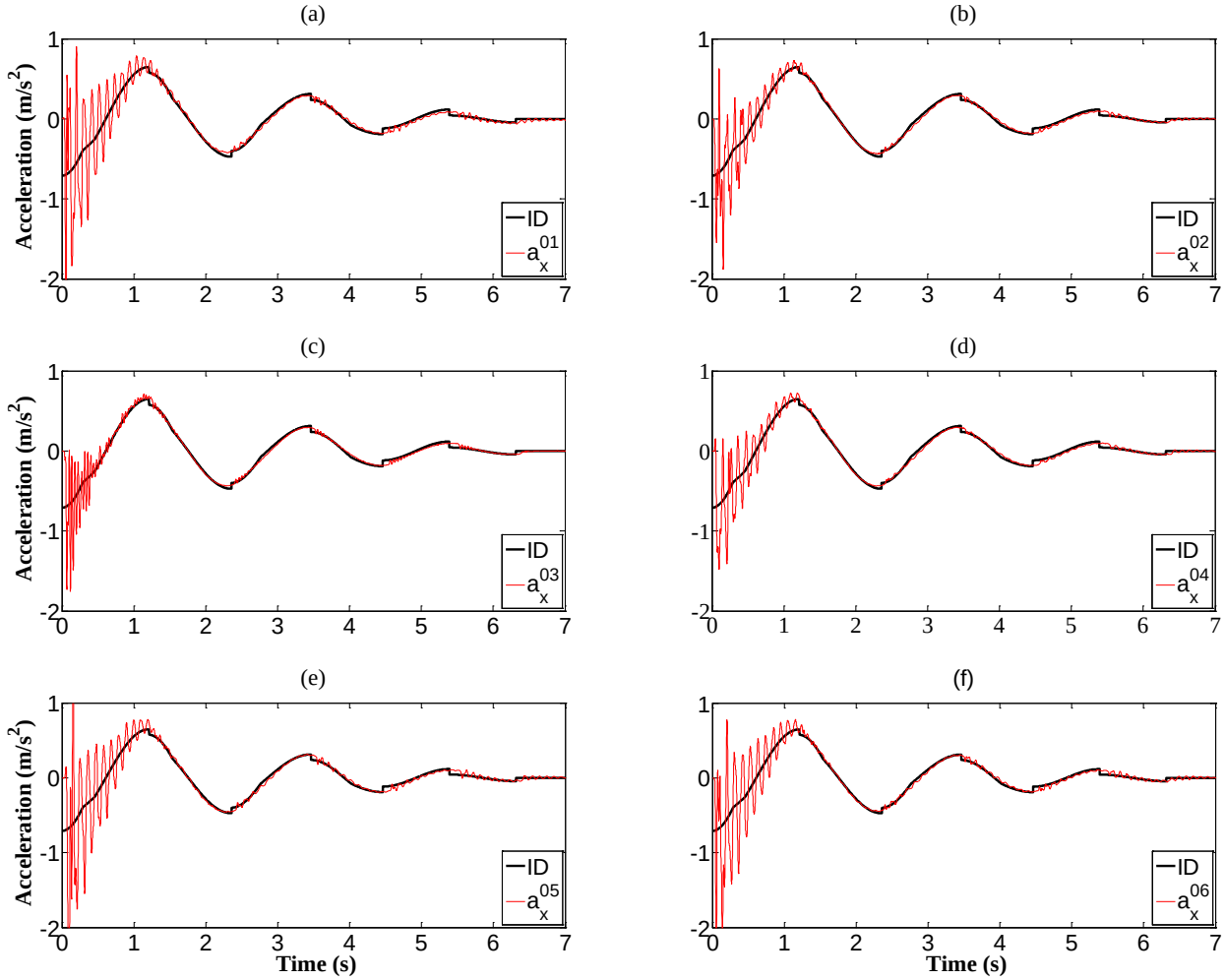


Fig. 3 - Simulated acceleration for Test 5 using THM and CCFM, and comparison with longitudinal accelerations recorded by transducers 01, 02, 03 ,04 ,05 ,06 at stations S1, S3, S4, S5, S6, S7.

Table 1 – Identified parameters for THM and BHM

| Model | $u_0$ (m) | | | | | LFSBs | | HDRBs | | | | |
|---|---|---|---|---|---|---|---|---|---|---|---|---|
| | Test 3 | Test 5 | Test 6 | Test 7 | Test 8 | $u_{d0}$ (m) | $r_{d0}$ | $u_y$ (m) | $u_B$ (m) | $f_0$ (Hz) | $f_1$ (Hz) | $f_2$ (Hz) |
| THM | 0.104 | 0.113 | 0.110 | 0.086 | 0.089 | 0.0032 | - | 0.014 | 0.080 | 0.540 | 0.416 | 0.323 |
| BHM | 0.115 | 0.124 | 0.120 | 0.095 | 0.100 | 0.0033 | 0.002 | 0.018 | - | 0.525 | 0.394 | - |

It may be useful to notice that for the CCFM, the only required parameter is $u_{d0}$, while for the BHM, the second yield displacement $u_B$, and the third characteristic frequency $f_2$, are not required.

The two sets of parameters given in Table 1 can be used to simulate the acceleration of the rigid superstructure. The acceleration computed for Test 5, using the THM and the CCFM, is shown in Fig. 3 and compared with the longitudinal acceleration recorded at the stations displayed in Fig. 2. It may be noticed that the simulated acceleration fits very well the long wave of the isolation mode while, as expected, it fails to capture the high frequency components associated with the deformation of the superstructure. Similar results are obtained by using the BHM and either the CCFM or the LCFM, but the fitting is somewhat less accurate. To show that the identified set of parameters provides a good fit for all the other tests also, the simulated acceleration for Tests 3, 6, 7, 8 is shown in Fig. 4, when using the THM and the CCFM, and compared with the acceleration recorded at station S6 by transducer 04.

The total reaction of the isolation system to the motion of the rigid superstructure in Test 5 is shown in Fig. 5. The HDRB and LFSB components, modeled by the THM and the CCFM respectively, are also shown in the figure. It may be interesting to notice how the contribution of the LFSB component to the total reaction is rather small overall, but becomes relevant when the amplitude of motion is small.

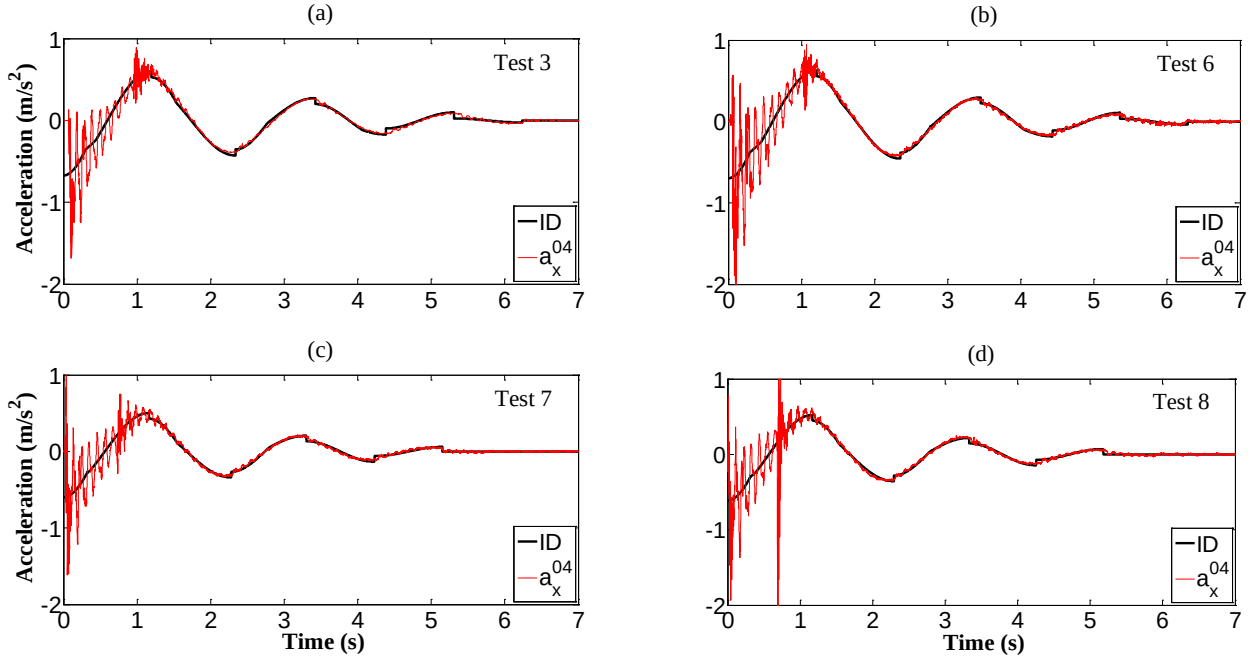


Fig. 4 – Simulated longitudinal acceleration for rigid superstructure for Tests 3, 6, 7, 8 using THM and CCFM, and comparison with acceleration recorded by transducer 04 at station S6.

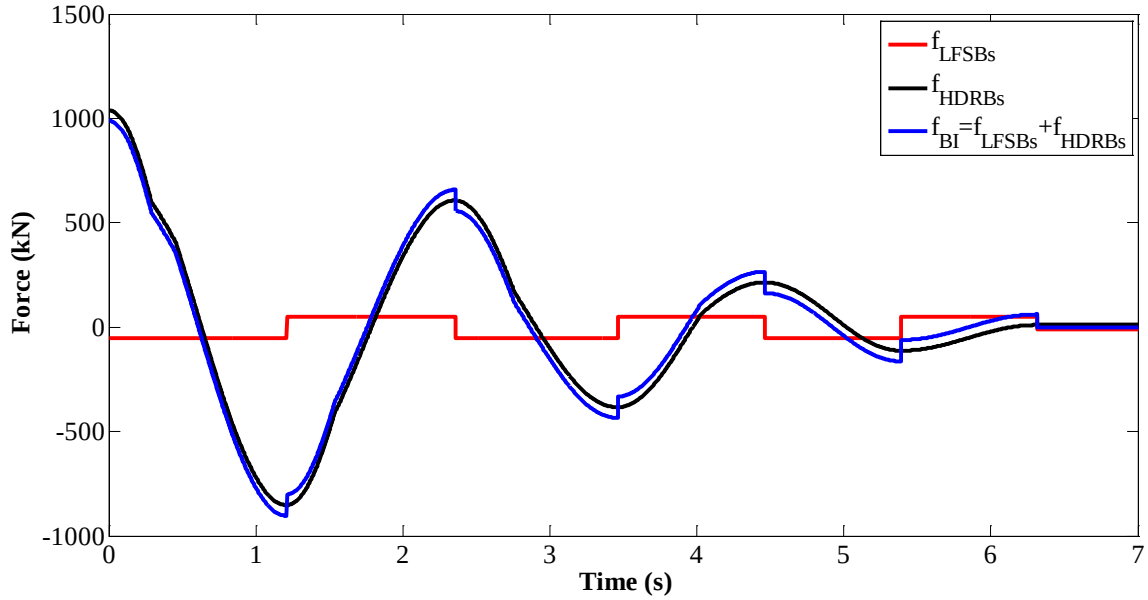


Fig. 5 – Simulation of the reaction force of the isolation system in Test 5. Total reaction (blue line) decomposed in the HDRB (black line) and LFSB (red line) components.

## 3. Modeling the superstructure

A detailed model of the superstructure was developed using the structural analysis software SAP2000. In this model, the supports consisting of the HDRBs and LFSBs were removed, and the superstructure was considered as a free body. The total number of nodes was 1985, and the total number of degrees of freedom, after introduction of in-plane rigid floor slab conditions, was 7694. Four-node shell elements were used to model membrane and plate-bending behavior of the stiffening walls. Three-dimensional frame elements accounting for biaxial bending, torsion, axial deformation and biaxial shear, were used for beam-column elements. For the evaluation of stiffness properties, the gross section properties were used. Because the structure is composed of structural concrete of different epochs, i.e. the original structure was constructed in the late '70s and the stiffening thin walls were built during the seismic retrofitting of 2003-2004, the elastic modulus of concrete was evaluated by the designer, according to the structural provisions of the time, through the formula $E_c = 5700\sqrt{R_{ck}}$. The cubic strength of the concrete, measured through tests, turned out to be 13MPa for the older structural elements, and 34MPa for the new ones. Condensed mass and stiffness matrices were constructed using the SAP2000 structural model. The diagonal mass matrix evaluated in the test conditions by considering the ten degrees of freedom associated with the hypothesis of rigid in-plane floor diaphragms, i.e. two degrees of freedom per floor being the building symmetric about the transverse axis, is given in Table 2.

Table 2 – Floor masses and rotational inertias for the Solarino building

| floor | ground | 1st | 2nd | 3rd | 4th |
|---|---|---|---|---|---|
| $m_x$ (kNs$^2$/m) | 422.49 | 255.11 | 243.30 | 240.58 | 223.10 |
| $I_z$ (kNs$^2$m) | 28748.21 | 17761.99 | 16657.38 | 16504.34 | 13765.39 |

Table 3 – Condensed stiffness matrix for the superstructure

| | | | | |
|---|---|---|---|---|
| **$K_{tt}$ [kN/m]** | | | | |
| 8444872 | -9087500 | 576128 | 25924 | 40578 |
| -9087500 | 17309668 | -8954021 | 567817 | 164039 |
| 576128 | -8954021 | 16582807 | -8964305 | 759394 |
| 25924 | 567817 | -8964305 | 16161822 | -7791256 |
| 40578 | 164039 | 759394 | -7791256 | 6827248 |
| **$K_{t\theta}$ [kN]** | | | | |
| 820238 | -1393616 | -829792 | -102125 | 644347 |
| -1423093 | 7771787 | -5576498 | -406438 | -389699 |
| -3554122 | -643756 | 13731394 | -9168284 | 405880 |
| 2642891 | -5455624 | -5766480 | 18356158 | -8098010 |
| 1514089 | -278788 | -1558622 | -8679309 | 7437485 |
| **$K_{\theta\theta}$ [kNm]** | | | | |
| 2123465384 | -2324227030 | 51752513 | 230710943 | -82060363 |
| -2324227030 | 3317052940 | -1076881195 | -107118395 | 190624325 |
| 51752513 | -1076881195 | 2045816905 | -1275664910 | 256187411 |
| 230710943 | -107118395 | -1275664910 | 2054785539 | -900688071 |
| -82060363 | 190624325 | 256187411 | -900688071 | 534161828 |

By using the SAP2000 detailed model, and by applying one force at a time to each of the considered degrees of freedom, a condensed flexibility matrix was constructed. The condensed stiffness matrix shown in Table 3 was then obtained by inverting the flexibility matrix.

## 4. Input motion to the superstructure

Because the structure is nearly symmetric with respect to the y axis, the input motion to the superstructure is specified in terms of the longitudinal acceleration of the center of mass of the floor just above the isolation system and by the rotational acceleration about the vertical axis through the same point. As shown in Fig. 6 and Fig. 2, there are 4 horizontal acceleration transducers in the floor just above the isolation system, but only three signals are required to evaluate the three components of motion at the center of mass. By using three signals at a time in 4 different combinations, it turned out that the results were more or less equal and that the transverse components were negligible compared to the longitudinal ones. However, in order to minimize experimental and modeling errors, it was decided to use the average of the four computations as input motion.

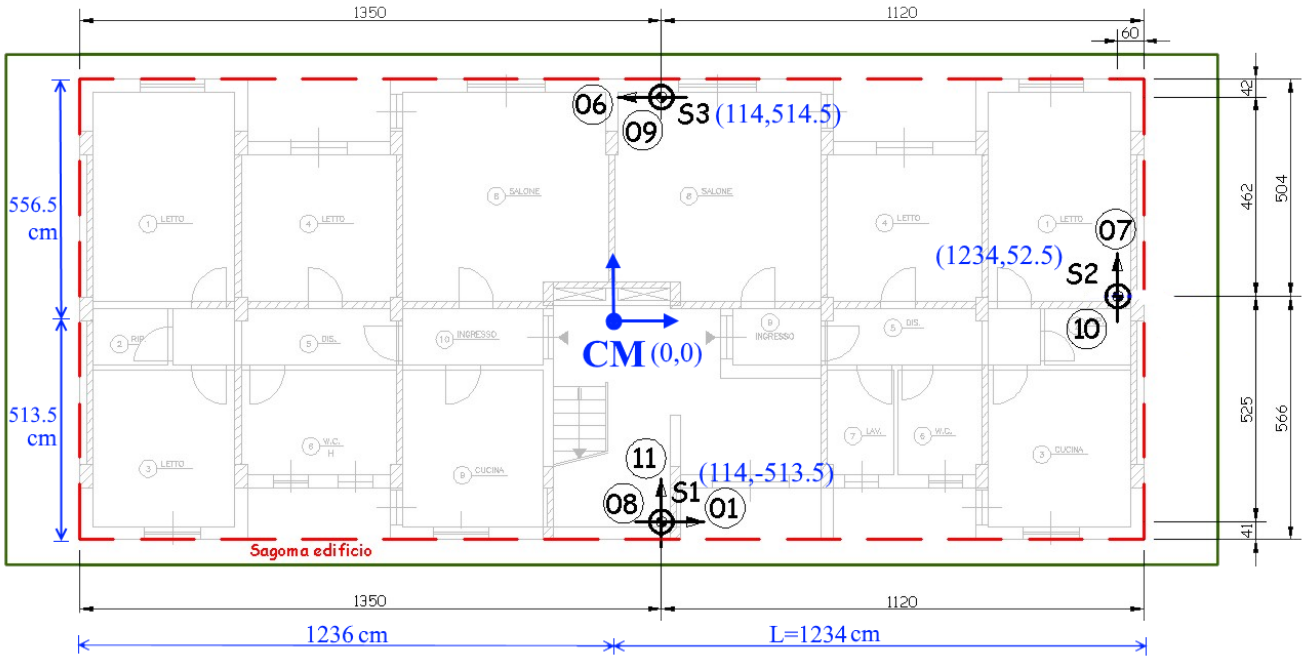


Fig. 6 – Layout of acceleration transducers on the floor just above the isolation system.

## 5. Equations of motion for the superstructure

The equations of motion for the superstructure may be written in partitioned form as follows:

$$\begin{bmatrix} \mathbf{M} & \mathbf{M}_b \\ \mathbf{M}_b^T & \mathbf{M}_{bb} \end{bmatrix} \begin{bmatrix} \ddot{\mathbf{u}}^t \\ \ddot{\mathbf{u}}_b \end{bmatrix} + \begin{bmatrix} \mathbf{C} & \mathbf{C}_b \\ \mathbf{C}_b^T & \mathbf{C}_{bb} \end{bmatrix} \begin{bmatrix} \dot{\mathbf{u}}^t \\ \dot{\mathbf{u}}_b \end{bmatrix} + \begin{bmatrix} \mathbf{K} & \mathbf{K}_b \\ \mathbf{K}_b^T & \mathbf{K}_{bb} \end{bmatrix} \begin{bmatrix} \mathbf{u}^t \\ \mathbf{u}_b \end{bmatrix} = \begin{bmatrix} \mathbf{0} \\ \mathbf{p}_b \end{bmatrix} \tag{2}$$

where $\mathbf{u}^t$ is the vector referring to the unknown degrees of freedom above the base floor, $\mathbf{u}_b$ is the input motion vector described in the previous paragraph, and $\mathbf{p}_b$ is the force imparted by the isolation system on the superstructure. Following Chopra [9], the vector of total displacements, $\mathbf{u}^t$, can be decomposed as the sum of the quasi static displacement, $\mathbf{u}^s$, and the dynamic displacement, $\mathbf{u}$, where $\mathbf{u}^s$ satisfies the static equation:

$$\mathbf{K}\,\mathbf{u}^s + \mathbf{K}_b\,\mathbf{u}_b = \mathbf{0} \tag{3}$$

The equation of motion for the superstructure therefore becomes:

$$\mathbf{M}\,\ddot{\mathbf{u}} + \mathbf{C}\,\dot{\mathbf{u}} + \mathbf{K}\,\mathbf{u} = -\left(\mathbf{M}\,\ddot{\mathbf{u}}^s + \mathbf{M}_b\,\ddot{\mathbf{u}}_b\right) - \left(\mathbf{C}\,\dot{\mathbf{u}}^s + \mathbf{C}_b\,\dot{\mathbf{u}}_b\right) \tag{4}$$

Assuming that damping is stiffness proportional, and using Eq. (3), Eq. (4) becomes:

$$\mathbf{M}\,\ddot{\mathbf{u}} + \mathbf{C}\,\dot{\mathbf{u}} + \mathbf{K}\,\mathbf{u} = -\left(\mathbf{M}_b - \mathbf{M}\,\mathbf{K}^{-1}\,\mathbf{K}_b\right)\ddot{\mathbf{u}}_b \tag{5}$$

The solution of Eq. (5) can be pursued advantageously by modal decomposition and synthesis.

The second of Eqs. (2) provides the forces that the isolation system applies to the superstructure. These can be given the following form:

$$\mathbf{p}_b = \mathbf{M}_b^T\ddot{\mathbf{u}}^t + \mathbf{M}_{bb}\ddot{\mathbf{u}}_b + \mathbf{C}_b^T\dot{\mathbf{u}}^t + \mathbf{C}_{bb}\dot{\mathbf{u}}_b + \mathbf{K}_b^T\mathbf{u}^t + \mathbf{K}_{bb}\mathbf{u}_b \tag{6}$$

## 6. Identification of the superstructure

Eq. (5) can be solved for **u**, and the total displacement $\mathbf{u}^t$ can be calculated by adding to **u** the quasi static displacement $\mathbf{u}^s$. Calculation of the total acceleration $\ddot{\mathbf{u}}^t$ is achieved in the same way. This allows for the calculation of the acceleration at all the measuring stations shown in Fig. 2, and for comparison with the accelerations measured during the tests. If the model were exact and its parameters tuned properly, the calculated accelerations would match the experimental measurements. However, in general neither the model can be totally exhaustive nor the parameters can be perfectly calibrated. In the following, using the best model available at this time, the system parameters shall be adjusted to obtain the best fit between simulated and measured accelerations. Two main assumptions shall be made concerning the stiffness and damping matrices of the superstructure: (i) the stiffness matrix can change only proportionally to a single parameter $\lambda_k$ and (ii) the damping matrix is proportional to the stiffness matrix through a parameter $\lambda_c$, so that only one damping parameter needs to be identified. Furthermore, it is assumed that the mass matrix generated via the SAP2000 software is sufficiently accurate. Therefore, equation of motion (5) can be written in terms of the unknown parameters $\lambda_k$ and $\lambda_c$ as follows:

$$\mathbf{M}\ddot{\mathbf{u}} + \lambda_c \lambda_k \mathbf{K}\dot{\mathbf{u}} + \lambda_k \mathbf{K}\mathbf{u} = -\left(\mathbf{M}_\mathbf{b} - \mathbf{M}\lambda_k^{-1}\mathbf{K}^{-1}\lambda_k \mathbf{K}_\mathbf{b}\right)\ddot{\mathbf{u}}_\mathbf{b} = -\left(\mathbf{M}_\mathbf{b} - \mathbf{M}\mathbf{K}^{-1}\mathbf{K}_\mathbf{b}\right)\ddot{\mathbf{u}}_\mathbf{b} \tag{7}$$

The un-damped free vibration modes associated with Eq. (5) are independent of the value of $\lambda_k$, while the corresponding frequencies $\omega_{k,n}$ are related to the frequencies $\omega_{1,n}$, associated with $\lambda_k = 1$, through the relationship $\omega_{k,n} = \omega_{1,n}\sqrt{\lambda_k}$. The damping ratios associated to each mode take the simple form $\zeta_{k,n} = \lambda_c \lambda_k \omega_{k,n}/2$.

The CMA-ES optimization algorithm was used, in the same form as explained in [7], for the identification of the unknown parameters $\lambda_c$ and $\lambda_k$. After ten runs, with population doubling after each run, the values of the parameters given in Table 4 were found from identification of Test 5.

Table 4 – Frequencies and damping ratios calculated from the identified parameters $\lambda_c = 0.0242$ and $\lambda_k = 0.3387$ using data from test 5

| mode | 1 | 2 | 3 | 4 | 5 | 6 | 7 | 8 |
|---|---|---|---|---|---|---|---|---|
| f [Hz] | 4.53 | 5.52 | 15.45 | 19.45 | 25.61 | 32.52 | 39.86 | 45.74 |
| $\zeta$ | 0.12 | 0.14 | 0.40 | 0.50 | 0.66 | 0.84 | 1.03 | 1.18 |

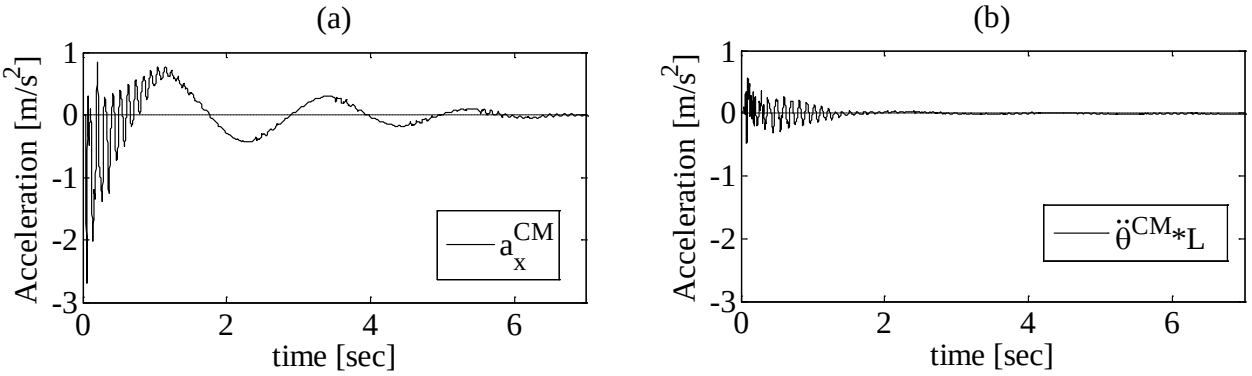


Fig. 7 - Input motion to the superstructure under Test 5, (a) longitudinal acceleration at the center of mass and (b) transverse acceleration at station S2-07 due to rotational acceleration $\ddot{\theta}^{CM}$ at the CM.

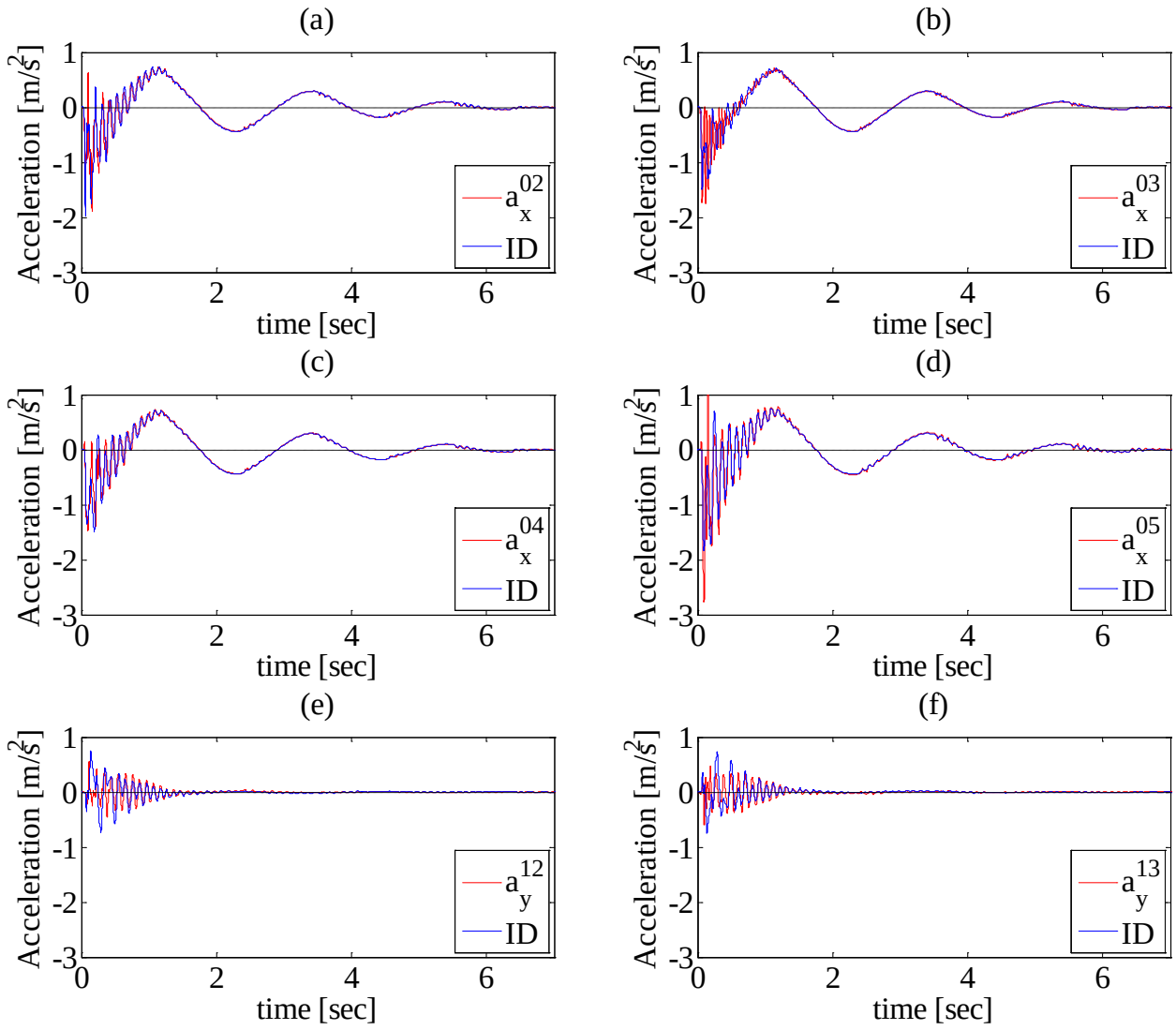


Fig. 8 - Simulated accelerations under Test 5 using the identified superstructure properties, and comparison with accelerations recorded by transducers 02, 03, 04, 05, 12, 13 at stations S4, S5, S6, S7, and S8.

The input motion used for the identification of the superstructure properties is shown in Fig. 7, where in (a) is the longitudinal acceleration at the center of mass while in (b) is the transverse motion at station S2-07 due to the rotational acceleration at the center of mass. Comparison of the signals in (a) and (b) gives a measure of the significance of the rotational motion. The total accelerations at all the recording stations in the superstructure were computed and compared in Fig. 8 with the recorded accelerations. The match is not perfect but the general trend and peak values are obtained to a good level of accuracy. With the same structural data in Table 3, the simulations of test 3, 6, 7 and 8 have been run obtaining the same level of accuracy as shown for test 5.

## 7. The reaction of the isolation system on the superstructure

The reaction of the isolation system on the superstructure can be calculated by using Eq. (6). To this purpose, velocities and displacements at the considered degrees of freedom are needed in addition to accelerations. These were obtained via numerical integration, following adequate filtering, and the procedure detailed in [10]. With reference to test 5 and to the base floor, velocities and displacements are shown in Figs. 9 and 10. With displacements and rotations at the considered degrees of freedom, the reaction vector of the isolation system can be calculated, and for test 5 the result is shown in Fig. 11. Superimposed to the horizontal reaction is the

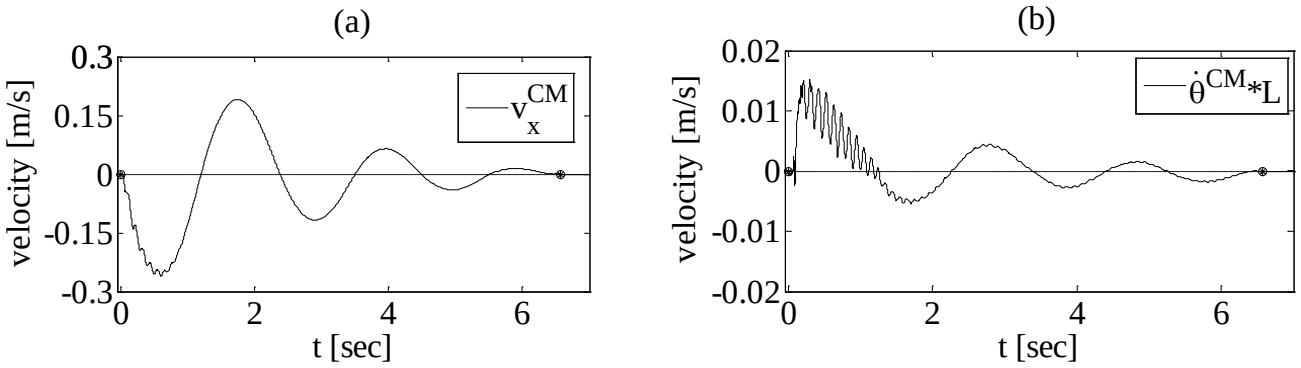


Fig. 9 - Input motion to the superstructure under Test 5, (a) longitudinal velocity at the center of mass and (b) transverse velocity at station S2-07 due to rotational acceleration $\ddot{\theta}^{CM}$ at the CM.

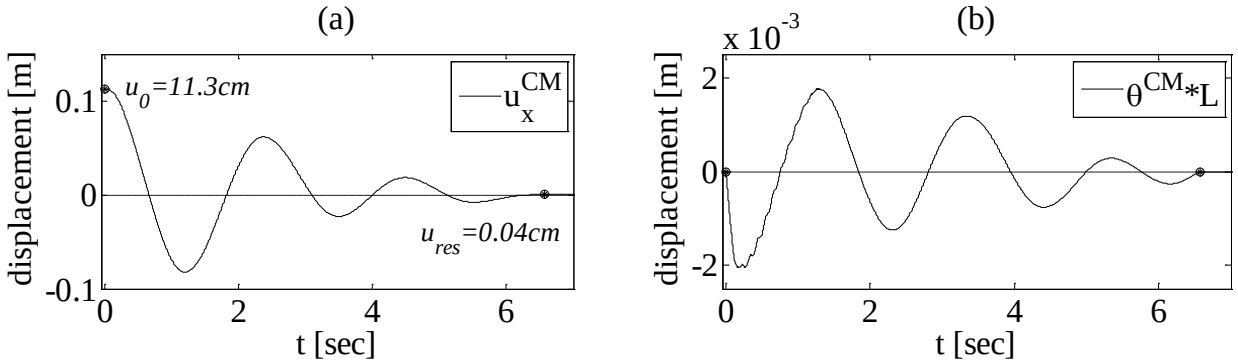


Fig. 10 - Input motion to the superstructure under Test 5, (a) longitudinal displacement at the center of mass and (b) transverse displacement at station S2-07 due to rotational acceleration $\ddot{\theta}^{CM}$ at the CM.

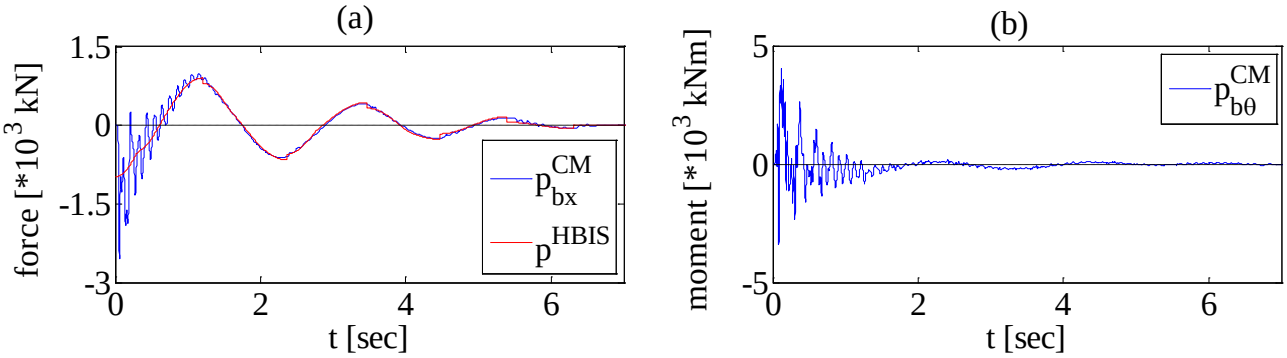


Fig. 11 – (a) Translational and (b) rotational reaction of the isolation system on the superstructure.

evaluation made by using the hypothesis of rigid superstructure and the one degree of freedom model. The translational force of the SDOF model fits well on average but totally misses the high frequency response. Obviously, no rotational reaction can be provided by the SDOF model.

## 8. Discussion

Simulations of the tests performed on the Solarino building have been attempted by using the SAP2000 model with properties for the isolators as specified in Table 1, and properties of the superstructure as given by

parameters $\lambda_c$ and $\lambda_k$ in Table 4. The results showed that the high frequency response was not captured. An explanation for

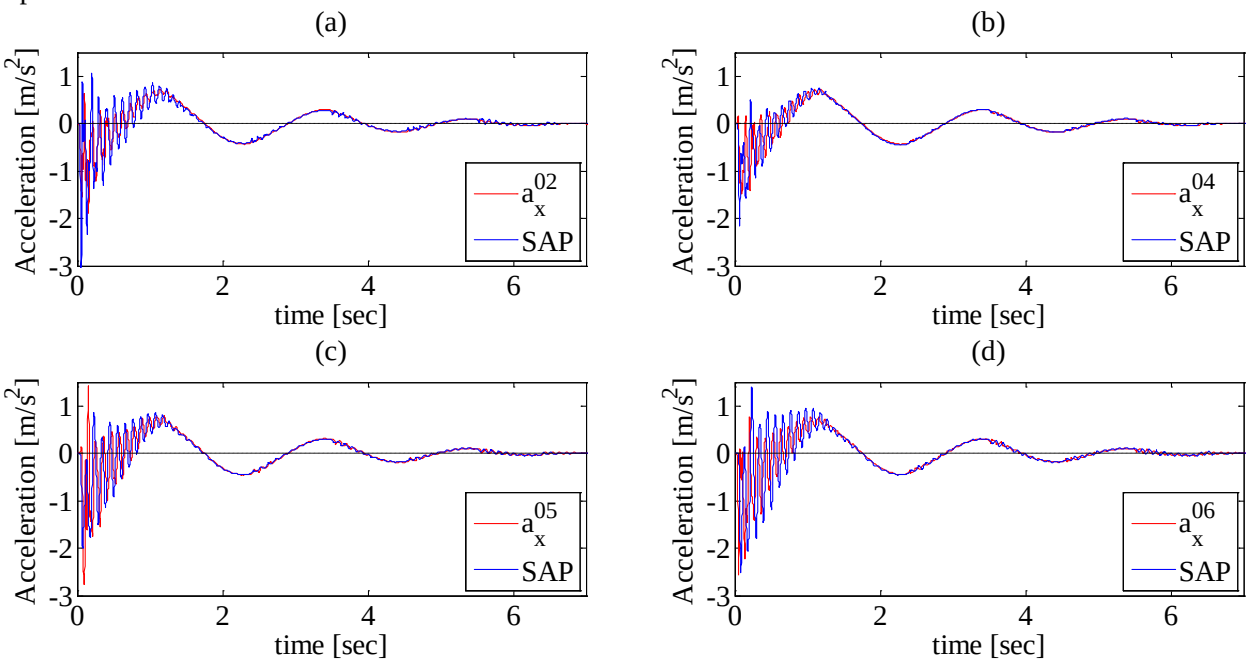


Fig. 12 - Simulated accelerations under Test 5 using the identified superstructure properties in SAP2000 free-body model, and comparison with measured accelerations recorded by transducers 02, 04, 05, 06 at stations S4, S6, S7 and S3.

this behavior may be found in the comparison of the reaction of the isolation system on the superstructure estimated by the SDOF model as given in Fig. 5, and the one calculated using Eq. (6), shown in Fig. 11. From Fig. 11(a) it may be seen that there is a strong high frequency component in the longitudinal force, calculated using Eq. (6), which is missing in the approximate evaluation shown in Fig. 5. The missing rotational component may be an additional reason for the observed mismatch. The unrealistic hypothesis of stiffness proportional damping was made in order to facilitate the convergence of the optimization algorithm and also in the belief that the high frequency components provided little contribution, if any, to the response. The damping ratios for the modes providing the largest contribution to the response were 12% and 14% respectively. These values may appear to be rather large, perhaps too large. However, one should consider that the peak recorded acceleration is of the order of 0.3g, if not larger. This is of the order of magnitude of accelerations recorded in buildings during major earthquakes and for which large values of the damping ratio have been estimated by researchers [9,11]. In the present case, the peak acceleration occurs in the initial phase of motion; it may be possible that, in order for this acceleration to rapidly damp out, as shown by the recorded signals, large values of the damping ratio are required.

If the reaction of the isolation system on the superstructure, computed using Eq. (6) and shown in blue in Fig. 11, is applied in the free-body SAP2000 model at the centre of mass of the base floor of the superstructure, the match between simulated and recorded accelerations is rather good, Fig.12. The stiffness multiplier $\lambda_k$ points to a significant reduction in stiffness of the system as calculated from gross section properties and code specifications for the elastic modulus of concrete [12]. Although a reduction of 50% is recommended by the same code, the identification procedure leads in this case to a stiffness reduction of about 66%.

## 9. Conclusions

The main contribution of the present work is the simultaneous identification of the superstructure properties and reactions of the isolation system. Contrary to previous simplified studies by the authors, the reactions of the

isolation system show a significant torsional component and high frequency content in both force and moment. The former may be easily explained with the lack of symmetry of the building along the longitudinal axis while the latter may be reasonably explained by interaction with the superstructure. A detailed model of the superstructure using SAP 2000 enables to establish, with sufficient reliability, the condensed mass matrix of the simplified dynamic model in the testing conditions. The structure of the stiffness matrix of the model used in the dynamic identification has been derived using the same detailed SAP2000 model but has been scaled via an optimization algorithm for the simulated response to match the experimental one. The assumption of stiffness proportional damping has been justified by the need to contain to a minimum the number of optimization parameters and also by the belief that higher modes provide little contribution to the structural response. The resulting high values of damping ratios, even in lower modes, may be justified by the high acceleration response in the early stages of motion and its subsequent rapid decay. A challenge for future research is to develop a model for the isolation system that enables a simulation of the release tests which is consistent with the identified reaction response derived in the present work.

## 10. Acknowledgements

This work was performed with the financial support of ReLUIS (Italian National Network of University Earthquake Engineering Laboratories), 'Project D.P.C-ReLUIS 2014–2016, WP1'

## 11. References

[1] Oliveto G, Calio I, Marletta M (2004): Retrofitting of reinforced concrete buildings not designed to withstand seismic action: a case study using base isolation. *13th World Conference on Earthquake Engineering*, Vancouver, Canada.

[2] Oliveto G, Granata M, Buda G, Sciacca P (2004): Preliminary results from full-scale free vibration tests on a four story reinforced concrete building after seismic rehabilitation by base isolation. *JSSI 10th Anniversary Symposium on Performance of Response Controlled Buildings*, Yokohama, Japan.

[3] Oliveto ND, Scalia G, Oliveto G (2010): Time domain identification of hybrid base isolation systems using free vibration tests. *Earthquake Engineering & Structural Dynamics*, **39** (9), 1015-1038.

[4] Oliveto G, Athanasiou A, Oliveto ND (2012): Analytical earthquake response of 1D hybrid base isolation systems. *Soil Dynamics and Earthquake Engineering*, **43**, 1–15.

[5] Oliveto ND, Athanasiou A, Oliveto G (2012): Mixed Lagrangian Formulation for dynamic and earthquake response of 2D hybrid base isolation systems. *9CUEE & 4ACEE Joint Conference: 9th International Conference on Urban Earthquake Engineering & 4th Asia Conference on Earthquake Engineering.* Centre for Urban Earthquake Engineering, Tokyo Institute of Technology, Japan.

[6] Oliveto G, Oliveto ND, Athanasiou A (2014): Constrained optimization for 1-D dynamic and earthquake response analysis of hybrid base-isolation systems. *Soil Dynamics and Earthquake Engineering*, **67**, 44-53.

[7] Markou AA, Oliveto G, Athanasiou A (2016): Response simulation of hybrid base isolation systems under earthquake excitation. *Soil Dynamics and Earthquake Engineering*, **84**, 120–133.

[8] Markou AA, Oliveto G, Athanasiou A (2012): Recent advances in dynamic identification and response simulation of hybrid base isolation systems. *15th World Conference on Earthquake Engineering*. Lisbon, Portugal, Paper No 3023.

[9] Chopra A (2012): *Dynamics of Structures. Theory and Applications to Earthquake Engineering.* Pearson, Prentice Hall, New Jersey, 4th edition.

[10] Athanasiou A (2016): *Dynamic identification of the Augusta hybrid base isolated building using data from full scale push and sudden release tests*. PhD thesis, University of Catania. DOI: 10.13140/RG.2.1.3625.3521.

[11] Goel RK, Chopra AK (1997b): Vibration properties of buildings determined from recorded earthquake motions. *Report No. UCB/EERC-97/14*, Earthquake Engineering Research Center, University of California, Berkeley, USA.

[12] NTC08 Norme Tecniche per le Costruzioni (2008): DECRETO 14 gennaio 2008, GU Serie Generale n.29 del 4-2-2008 - Suppl. Ordinario n. 30.